

# ELECTRON CLOUD EFFECT IN DAMPING RINGS OF LINEAR COLLIDERS

K. Ohmi\*

KEK, Oho, Tsukuba, Ibaraki, 305-0801, Japan

## Abstract

Damping rings of Linear Colliders are very low emittance ( $\varepsilon_x < 1$  nm) and high current ( $I \sim 1$  A) storage rings which accumulate electron and positron during several damping times. The positron damping ring seems to be serious for electron cloud instability obviously. We discuss electron cloud build-up, coupled and single bunch instabilities for the damping rings of GLC/NLC and TESLA.

## INTRODUCTION

Design of Linear Collider projects are in progress as a world wide collaboration. There are two possibility for the linear collider scheme: one is normal conducting cavity with X/C band power source, and another is superconducting cavity with L band power source.

A positron damping ring storages positron beam during several damping time and extracts the beam with a very low emittance to a main acceleration linac of the linear collider. The damping ring accumulates many positron bunches of the population of  $\sim 10^{10}$  with a narrow spacing. The positron beam emits synchrotron radiation photons, which creates a large number of photoelectrons at the chamber surface. Though ante-chambers are used to avoid the photoelectrons, considerable rate of photoelectrons and secondary electrons are accumulated in the chamber. Study of the electron cloud effect in the damping ring is one of the most important subject to realize the linear collider.

Some works on the electron cloud effect (CLIC, NLC, TESLA and JLC) have been done for damping rings of linear collider projects as shown in Refs. [1, 2, 3, 4]. In this paper, studies of electron cloud build-up, coupled bunch and single bunch instabilities in GLC/NLC and TESLA damping rings are presented.

The parameters of damping rings are shown in Table 1. There are two parameters for the GLC/NLC damping ring, where I and II are old and present ones.

## ELECTRON CLOUD BUILD-UP

At first we investigate multipactoring threshold of electron cloud build-up. Above the threshold, a small number of electrons are amplified exponentially, with the result that final electron density, which does not depend on initial yield of electrons, is determined by a balance of beam-electron force and space charge force between electrons. In such case, the line density of electrons, which increases up

to neutralized level with that of beam, is too high to keep the beam with the design parameters.

When electrons are absorbed at the chamber wall surface, secondary electron emission is taken into account with the formula [5],

$$\begin{aligned} \delta_2(E) &= \delta_2(0) \exp(-5E/E_{\max}) \\ &+ \delta_{2,\max} \times \frac{E}{E_{\max}} \frac{1.44}{0.44 + (E/E_{\max})^{1.44}}, \end{aligned} \quad (1)$$

where  $E_{\max} = 300$  eV,  $\delta_2(0) = 0.5$ . The peak secondary yield ( $\delta_{2,\max}$ ), which depends on chamber material, is scanned between  $1.2 \sim 2.0$ .

We calculate electron density using the simulation code PEI [6]. Motions of electrons interacting with beam are tracked, and creation and absorption of electrons are reproduced on a computer. The distribution and the accumulated number of electrons in the vacuum chamber are obtained as a function of time. Space charge force between electrons is neglected in these calculations, since an amplification from a small number of electron is focused. Figure 1 shows the electron amplification, which is the number of accumulated electrons in a chamber normalized by the initial number. The amplification factor ( $A_e$ ) exponentially grows for time at high  $\delta_{2,\max}$ . The pulse (train) length of bunches is 270 ns (192 bunch  $\times$  1.4 ns for GLC/NLC, while bunches are filled every 20 ns (2820 bunches) in the TESLA damping ring. The amplification is 40 ( $\delta_{2,\max} = 1.2$ )  $\sim$  1000 ( $\delta_{2,\max} = 1.5$ ) for GLC/NLC. The amplification in bending magnets is worse than that of drift space. For TESLA the amplification is followed up to 4  $\mu$ s.  $\delta_{2,\max} \leq 1.8$  is no problem for drift space, but electrons are accumulated in the bending section even for  $\delta_{2,\max} = 1.7$ . These results were consistent with those given by M. Pivi et al. [4].

We next consider the primary yield of electron. Electrons are produced by ionization of residual gas due to positron beam. The electron production rate per a positron traveling in a meter is  $n_I \sim 1 \times 10^{-8} e^- / (m \cdot e^+)$  at  $2 \times 10^{-7}$  Pa.

Positron loss at chamber creates electrons, but the loss rate is very small. If the beam life time is 1 hour, the loss rate is  $n_L = 10^{-12} e^+ / (m \cdot e^+) Y_e$ . It does not seem to be large, depending on the conversion efficiency of  $e^+$  to  $e^-$ ,  $Y_e$ .

The photo-emission due to synchrotron radiation is further dominant from the above two sources. The number of photon hitting the chamber wall is given by

$$n_\gamma / (m \cdot e^+) = \frac{5\pi}{\sqrt{3}} \frac{\alpha\gamma}{L}, \quad (2)$$

\* ohmi@post.kek.jp

Table 1: Basic parameters of the GLC/NLC and TESLA damping rings

		GLC/NLC-I	GLC/NLC-II	TESLA
circumference	$L$ (m)	348.3	300	17,000
energy	$E$	1.98	1.98	5.
bunch population	$N_+$	$0.75 \times 10^{10}$	$0.75 \times 10^{10}$	$2 \times 10^{10}$
bunch spacing	$\ell_b$ (ns)	1.4	1.4	20
emittance	$\varepsilon_x$ (m)	$7 \times 10^{-10}$	$2.4 \times 10^{-10}$	$3 \times 10^{-10}$
	$\varepsilon_y$ (m)	$5 \times 10^{-12}$	$3.6 \times 10^{-12}$	$8 \times 10^{-13}$
typical beta function	$\beta$ (m)	10	10	35(H)/66(V)
bunch length	$\sigma_z$ (mm)	5	5.5	5.5
synchrotron tune	$\nu_s$	0.01	0.00118	0.066
beam pipe radius	$R$ (cm)	1.0	1.0	2.5

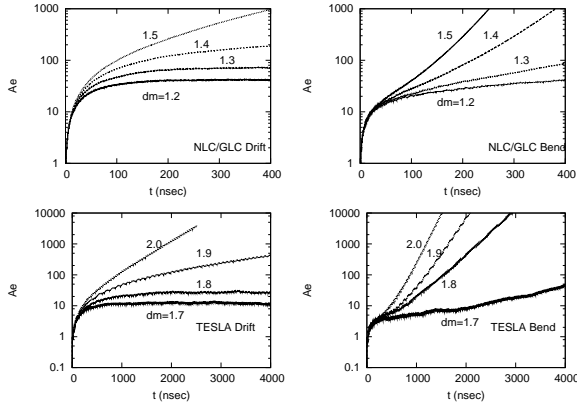


Figure 1: Amplification of electron cloud. The amplifications, which are the numbers of accumulated electrons normalized by those of initial electrons, for (a) GLC/NLC-II in drift space, (b) GLC/NLC-II in bending magnet, (c) TESLA in drift space, and (d) TESLA in bending magnet are depicted.

for a positron in a meter, where  $\alpha$  and  $\gamma$  are  $1/137$  and the relativistic factor, respectively. The photon hitting rate is  $n_\gamma = 0.65\gamma/(m \cdot e^+)$  for the GLC/NLC damping ring. The number of photo-electron produced by a positron at the chamber is given by

$$n_{e\gamma}(/m \cdot e^+) = n_\gamma Y_\gamma. \quad (3)$$

The direct photo-emission rate was estimated to be  $Y_\gamma = 0.1$  for cylindrical chamber. This value was consistent with an in situ measurement of electron current using button electrode in KEKB-LER [7]. The electron production rate due to photo-emission is  $n_{e\gamma} = 0.065e^-/(m \cdot e^+)$  per a positron traveling in a meter for the GLC/NLC damping ring ( $Y_\gamma = 0.1$ ). This value is 10 million bigger than that of ionization. If the electrons are accumulated  $A_e = 10$  times of the yield in the chamber, their density, which reaches to the neutralization level, is serious for the beam. The electron yield caused by the photo-emission must be reduced by an ante-chamber. The reduction rate depends on geo-

metrical design, where photons are absorbed.

A test ante-chamber made from copper was installed in KEKB-LER to investigate the density and yield of the electron cloud. Electrons detected by the monitor using button electrode were reduced to be  $1/100$  of the case of cylindrical copper chamber for low beam current  $< 100$  mA [8]. The reduction factor decreased to be  $1/5$  for high beam current  $> 1$  A. This decrease of the ratio seems to be due to that multipactoring gradually dominates at the higher beam current. From the detected electron at low current, it is conjectured that the antechamber protected 99% of electrons, produced by photo-emission at the KEKB test ante-chamber.

We evaluate electron cloud build up with a condition, the protection of primary electrons,  $99.5\% \sim 99\%$ , and the secondary peak yield,  $\delta_{2,\max} = 1.2$ . As is shown later, the condition is critical for the electron cloud instability in the GLC/NLC damping ring. The electron density is roughly estimated by the initial yield, the beam line density, the amplification and cross-section of the chamber as  $3.3 \times 10^{-4} \times 0.75 \times 10^{10} \times 30 / (0.42 \times 0.01^2 \pi) = 5.6 \times 10^{11} \text{ m}^{-3}$ , where 30 is the amplification ( $A_e$ ) shown in Figure 1(a). Simulation considering initial production rate is performed to obtain the cloud distribution and density in detail. Space charge force of electron cloud is taken into account in these calculations.

The electron production rate is now given by

$$n_{e\gamma} = 0.065 \times 0.005 - 0.01 / m \cdot e^+ = 3.3 - 6.6 \times 10^{-4} / m \cdot e^+. \quad (4)$$

The beam chamber is assumed to be cylindrical shape and electrons are produced uniformly along azimuthal angle with the reduced rate in the simulation.

Figure 2 shows variation of electron cloud density as a function of bunch passage in the GLC/NLC damping ring. Note that the unit of the horizontal axis corresponds to 1.4 ns. Averaged density of whole chamber and local density near beam are plotted. Pictures (a) and (b) shows the densities for 99% and 99.5% protection cases, respectively, in drift section, and (c) and (d) shows densities for the same cases in bending magnets. The central density is modulated

strongly by focusing of beam. The lowest value of each time (bunch) is the density, with which a bunch starts to interact the cloud, is used in the head-tail simulations. The density increases and saturates at a certain density in drift space, while does not saturate in bending magnet. Since the train length is limited to 192 bunches, the density is not very high in bending magnet. The central local density is lower than that in drift space, if anything. In bending magnet, electron motion is restricted along vertical direction, therefore the central density is not high. Depending on parameter, dense pillars of electrons are seen in a bending magnet [9]. Instabilities are evaluated mainly for drift section in following section, because of the higher densities. The saturated density is  $3 \times 10^{12} \text{ m}^{-3}$  and  $1.5 \times 10^{12} \text{ m}^{-3}$  for 99% and 99.5% protection, respectively, at center, and  $1.4 \times 10^{12} \text{ m}^{-3}$  and  $0.7 \times 10^{12} \text{ m}^{-3}$  for average. This value  $0.7 \times 10^{12} \text{ m}^{-3}$  is consistent with the simple estimation from the initial rate and the amplification factor,  $5.6 \times 10^{11} \text{ m}^{-3}$ , and therefore the density linearly depends on primary yield of 0.5% or 1%.

## COUPLED BUNCH INSTABILITY

The coupled bunch instability is caused by a long range ( $\sim \text{m}$ ) wake field, which is induced by the electron cloud. The wake field is evaluated as follows [6],

- Primary electrons are created in every bunch passage through the chamber center with the line density  $n_{e\gamma}$ . Secondary electrons are created at absorption of an electron with an energy ( $E_{abs}$ ) by the rate  $\delta_2(E_{abs})$ .
- The creation process is repeated until the cloud density saturate at a certain value. These two steps is the same is the build-up simulation.
- A bunch with a slight displacement passes through the cloud, and then following bunches without displacement pass through the chamber center.
- The creation process is repeated for the displaced and following bunches.
- The following bunches experience forces from the cloud, because the cloud is perturbed by the passage of the displaced bunch. The wake field is calculated by the forces.

Figure 3 shows the typical shape of the wake field (99 % protection). In the figure, 180-th bunch is displaced 1 mm and the average velocity kicks of electrons, which are related to the kick which bunches experience, are plotted. The wake field for drift space and bending magnet are depicted in pictures (a) and (b), respectively. The wake field in drift space has general feature of the transverse wake field: namely it is defocusing for small  $z$ , with the result that higher (or negative) modes ( $\omega \sim n\omega_0 - \omega_\beta$ , where  $0 < n < H/2$ ), are enhanced in the unstable spectrum. On the other hand, the wake in bending magnet has focusing nature for small  $z$ , especially in horizontal. In this case

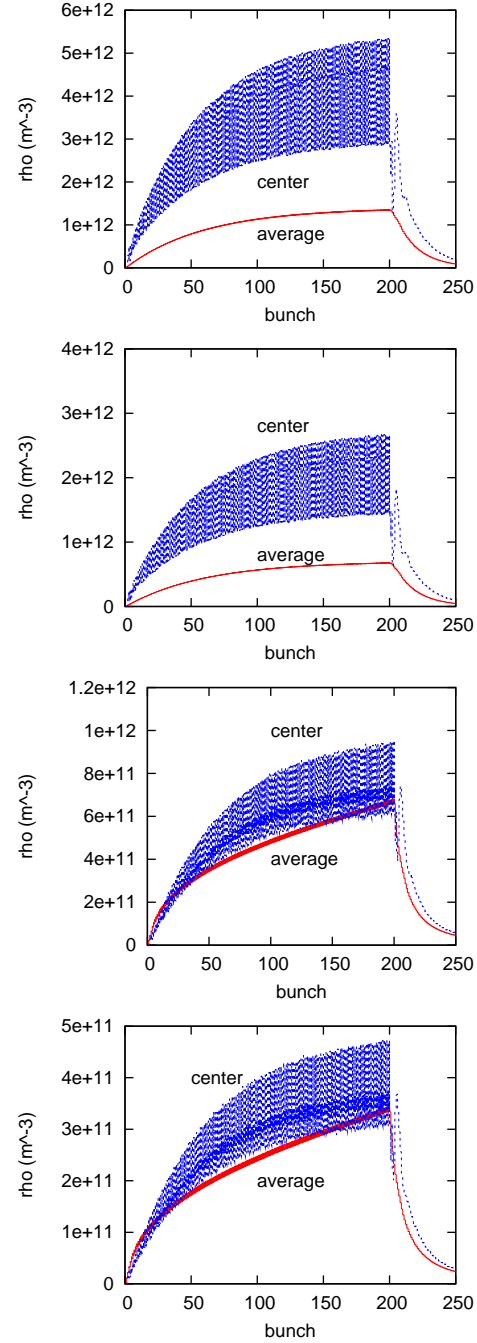


Figure 2: Electron cloud build-up in the GLC/NLC-II damping ring. Average and center cloud densities for (a) 99% and (b) 99.5% in drift space, and (c) 99% (d) 99.5% in bending magnet are depicted. The center cloud density is that of radius of 1 mm.

lower modes ( $\omega \sim n\omega_0 + \omega_\beta$ ) are enhanced (see Figure 4(b)). Similar feature is seen in mode spectrum with applying solenoid field [10].

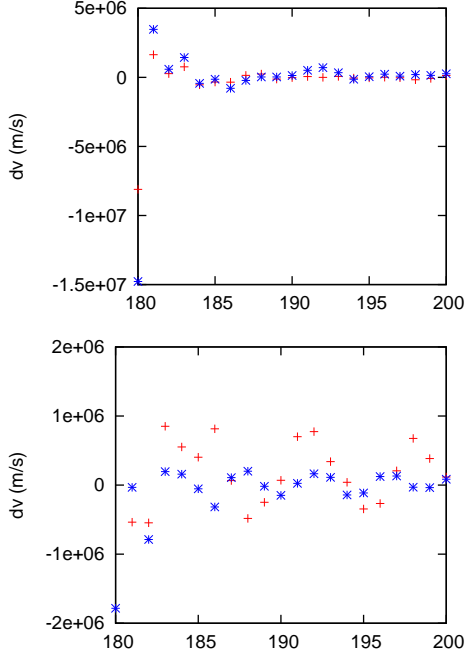


Figure 3: Long range wake field induced by the electron cloud. The wake field is represented by unit of velocity kick of electron cloud (m/s). Red and blue points are horizontal and vertical wake, respectively.

The growth rate of the coupled bunch instability is estimated by the formula

$$\Omega_m - \omega_\beta = \frac{N_e}{4\pi\gamma\nu_y N_p} \sum_{k=1}^n \frac{dv_{y,k}}{dy_0} e^{2\pi i k(m+\nu_y)/h}, \quad (5)$$

where  $N_e$  is the number of the photoelectron produced by a bunch through the ring circumference,  $N_p$  the number of positrons in a bunch,  $n$  the range of the wake field, and  $\gamma$  the Lorentz factor.  $dv_{y,k}/dy_0$  is the wake field for  $k$ -th bunch due to displacement of a bunch ( $y_0$ ) in unit of velocity kick of photoelectron cloud divided by the displacement. Figure 4 shows the growth of the coupled bunch mode caused by electron cloud. Mode spectra in drift space angle bending magnet are depicted in pictures (a) and (b), respectively. Modes with positive values are unstable in the figure. As is discussed above, higher order mode is unstable in drift space, and lower order mode is unstable in bending magnet. The growth rate in bending magnet is slower and occupation of the bending magnets is not much, therefore mode spectrum in drift space will be observed in experiments.

The growth rate was obtained as  $300\mu s$  (300 turn) and  $600\mu s$  (600 turn) for 99% and 99.5% protection, respectively. The coupled bunch instability can be cured by a bunch by bunch feedback system, which can have a damping time of  $100\mu m$  (100 turn). From these results, the

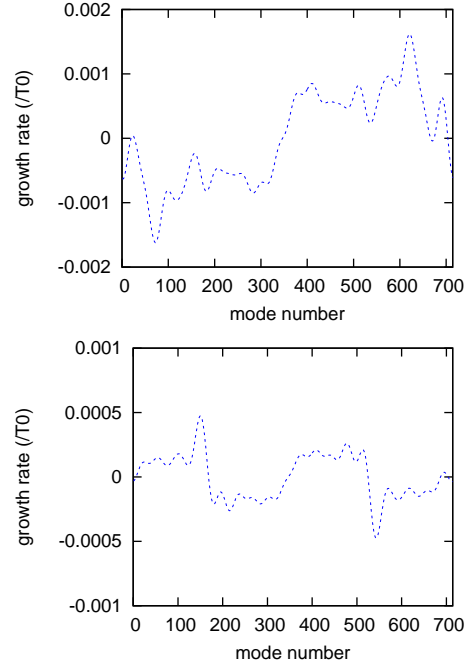


Figure 4: Growth rate for vertical coupled bunch instability caused by the electron cloud in the GLC/NLC-II damping ring. Mode spectra in drift space angle bending magnet are depicted in pictures (a) and (b), respectively.

electron (photon) protection rate is required to be less than 97% for  $\delta_{2,\max} = 1.2$  and 98.5% for  $\delta_{2,\max} = 1.3$  (see Figure 1(a). Note that the amplification factor is twice at  $\delta_{2,\max} = 1.3$ ).

## SINGLE BUNCH INSTABILITY

A single bunch instability is caused by a short range ( $\sim$  cm) wake field, which is induced by the electron cloud. The short range wake field can be analytically estimated by a simple model: that is, beam and electron cloud with the same transverse size interact with each other. We focus on the vertical instability in this paper. The wake field is represented by a resonator model. The resonator frequency ( $\omega_e$ ) corresponds to oscillation frequency of electrons in the beam field,

$$\omega_{e,y} = \sqrt{\frac{\lambda_+ r_e c^2}{\sigma_y (\sigma_x + \sigma_y)}}, \quad (6)$$

where  $\lambda_+$  and  $\sigma_{x(y)}$  are the beam line density in a bunch and transverse beam sizes, respectively.  $r_e$  and  $c$  are the electron classical radius and the speed of light, respectively. The wake field is expressed by

$$W_1(z) [\text{m}^{-2}] = c \frac{R_S}{Q} \sin\left(\frac{\omega_e}{c} z\right), \quad (7)$$

where

$$c \frac{R_S}{Q} = \frac{\lambda_e}{\lambda_+} \frac{L}{\sigma_y (\sigma_x + \sigma_y)} \frac{\omega_e}{c}. \quad (8)$$

The density of electron cloud  $\lambda_e$ , which is local line density near the beam, is related to the electron volume density  $\rho_e$  via  $\lambda_e = 2\pi\rho_e\sigma_x\sigma_y$ . In our parameters (GLC/NLC-I),

$$cR_S/Q = 0.94 \times 10^7 \text{ m}^{-2} \quad \omega_e = 5.5 \times 10^{11} \text{ s}^{-1}. \quad (9)$$

We can also estimate the wake field using numerical method. Electron cloud is much larger than beam size, non-linear force may be important and electrons are focused (pinched) at the beam center. The numerical calculation can take into account these effects partly. The wake field is calculated in a similar way as that for the coupled bunch instability. The beam is uniformly distributed along  $z$  direction, and as the initial condition the electron cloud is set to be a uniform distribution with a large transverse size ( $10\sigma_x \times 10\sigma_y$ ).

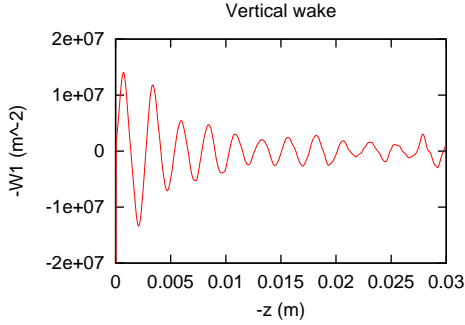


Figure 5: Short range wake field induced by the electron cloud.

Figure 5 shows the vertical wake field obtained by the simulation. The wake field in the figure damps along  $z$  due to nonlinear interaction with the electron cloud, though that in Eq.(7) does not damp, namely a finite  $Q$  factor is obtained. The figure shows a slightly larger  $cR_S/Q = 1.4 \times 10^7 \text{ m}^{-2}$  than the analytical value, and  $Q \sim 3$ .  $\omega_e$  is close to the analytical value.

The impedance due to the electron cloud is written as

$$Z(\omega) = \frac{cR_S}{\omega} \frac{1}{1 + iQ \left( \frac{\omega_e}{\omega} - \frac{\omega}{\omega_e} \right)} \quad (10)$$

$$= K \frac{\lambda_e}{\lambda_+ \sigma_y(\sigma_x + \sigma_y)} \frac{L}{\omega} \frac{\omega_e Z_0}{4\pi} \frac{Q}{1 + iQ \left( \frac{\omega_e}{\omega} - \frac{\omega}{\omega_e} \right)},$$

where  $K$  is an enhancement factor due to cloud size, pinching etc. [11], and  $Z_0$  is the impedance of vacuum ( $377\Omega$ ). The figure 4 shows  $K = 1.5$ . In the case of KEKB, the enhancement factor was  $K = 2 \sim 4$  for the vertical wake field.

The single bunch instability is estimated from the wake field. We use the coasting beam model to evaluate the instability, because of  $\omega_e\sigma_z/c \gg 1$ . The threshold of the

instability is expressed by

$$U \equiv \frac{\sqrt{3}\lambda_+ r_e \beta \omega_0}{\gamma \omega_e \eta \sigma_\delta} \frac{|Z_\perp(\omega_e)|}{Z_0} = \frac{\sqrt{3}\lambda_+ r_e \beta}{\gamma \nu_s \omega_e \sigma_z/c} \frac{|Z_\perp(\omega_e)|}{Z_0} = 1. \quad (11)$$

For  $U > 1$ , the beam is unstable.

We estimated the threshold value of electron cloud density for various positron storage rings,

$$\rho_{e,th} = \frac{2\gamma \nu_s \omega_e \sigma_z/c}{KQ\sqrt{3}r_e\beta L} \quad (12)$$

The results the damping rings are shown in Table 2.

Table 2: Single bunch electron cloud instability in positron storage rings. The enhancement factor is chosen to be  $K = 3$ . The impedance is evaluated at  $\rho_e = 10^{12} \text{ m}^{-3}$ .

variable (unit)	G(N)LC-I	G(N)LC-II	TESLA
$\omega_c\sigma_z/c$	9.1	13.3	13.0
$\rho_{e,th} (10^{12} \text{ m}^{-3})$	2.64	6.21	0.22
$\rho_{e,sim} (10^{12} \text{ m}^{-3})$		1.5	

The threshold density for the GLC/NLC damping ring is larger than the predicted cloud density ( $1.5 \times 10^{12} \text{ m}^{-3}$ ): that is, the single bunch instability does not occurs in the present condition.

Though the wake field approximated by the resonator model permits us to study the instability with simple analytic methods, the estimation of the threshold includes somewhat ambiguous factors: i.e., for example, how to choose  $K$  and  $Q$ . Since  $K$  is related to pinching, one may choose  $K \sim \omega_e\sigma_z/c$ . A value of  $Q$  which is larger than  $\omega_e\sigma_z/c$  is meaningless. To remove the ambiguity, tracking simulations are required.

Two types of simulations have been done to study the single bunch instability due to the electron cloud. One is simplified simulation, in which a positron bunch is represented by macro-particles distributed on the longitudinal phase space [12, 13, 14]. This model is a kind of extended two particle model, which is used for studying the head-tail effect due to ordinary impedance.

Another is more accurate model, in which a positron bunch and electron cloud are represented by many macro-particles. A bunch is divided into many ( $\sim 50$ ) longitudinal slices, and their interactions with cloud is evaluated by solving electric potential with particle in cell method. A code named PEHTS is used for the simulation [15]. The same method is used in the strong-strong simulation for studying the beam-beam effects. Detailed algorithm is presented in Ref.[16]. The same algorithm is used widely in the beam-beam, beam-ion and beam-cloud simulations [17, 18, 19, 20].

One typical single bunch instability mechanism is the head-tail effect. Though another mechanism, which is related to a large tune shift induced by electron cloud, may

be exist, the instability mechanism has been studied but is not clear yet [21]. Therefore we focus head-tail effect in this paper, though the other instability is seen in following results.

In the simulation, beam-electron interaction is estimated several times in one revolution of beam. The head-tail effect does not depend on tune basically except for a special tune. The instability is characterized by interaction strength per one synchrotron period. The interaction may be applied continuously or some discrete kicks. The difference is negligible if many kicks are applied in one synchrotron period. Since synchrotron tune is much less than 1, one kick per revolution is sufficient except for special tune with a synchro-beta resonance.

This fact means that the head-tail effect is scaled by integrated interaction (wake) strength divided by synchrotron phase advance: namely

$$\int \rho_e(s) ds / \int \phi(s)_s ds \sim \bar{\rho}_e / \nu_s. \quad (13)$$

If some kinds of phenomena deviate from the scaling, they are another kind of instability, otherwise they are false. We sometimes face the other instability than head-tail one in the simulations. The judgment whether true or false sometimes confuses. The typical case can be seen below.

The scenario of the head-tail instability is as follows. Motion of each particles in a bunch (cloud) moving in an electric potential of cloud (bunch) is calculated. Electrons, which oscillate with the frequency ( $\omega_e$  in Eq.(6)) causes variation of dipole moment of the bunch along  $z$ ,  $\langle y_+(z_i) \rangle$ , where  $z_i$  is the longitudinal position of  $i$ -th slice. Dipole moment of cloud  $\langle y_e(t = z_i/c) \rangle$  moves along the interaction of  $i$ -th slice of the bunch coherently with the frequency ( $\omega_e$ ). The beam size  $\langle y_+^2(z_i) \rangle$  grows due to smear of the dipole motion of beam.

We first present the simulation results for GLC/NLC-I damping ring. Figure 6 shows typical feature of the head-tail instability. Transverse dipole moment of a bunch and cloud along the longitudinal direction, and dipole moment of cloud are depicted in pictures (a) and (b) for  $\nu_s = 0$  and  $= 0.002$ .

Figure 7 shows growth of beam size for various cloud densities and various synchrotron tunes. pictures (a), (b), (c) and (d) are obtained for the cloud density,  $\rho_e = 1, 2, 5$ , and  $10 \times 10^{11} \text{ m}^{-3}$ , respectively. In each picture, evolutions for some synchrotron tunes are depicted. The threshold for the synchrotron tune is 0.001, 0.002, 0.005 and 0.01, respectively: that is, the threshold synchrotron tune is scaled by the density.

Figure 8 shows the scaling for  $\bar{\rho}_e / \nu_s$ . Evolutions for  $\rho_e / \nu_s = 1 \times 10^{11} / 0.001$  in the figure grids are depicted in this figure. For low cloud density less than  $5 \times 10^{11} \text{ m}^{-3}$ , the evolutions of the beam size have good agreement each other. The growth for  $\rho_e = 1 \times 10^{12} \text{ m}^{-3}$  deviates from others. The deviation are not explained by the head-tail effect. It is due to that electrons are localized in the simulation. If actual distribution is localized, we may observe

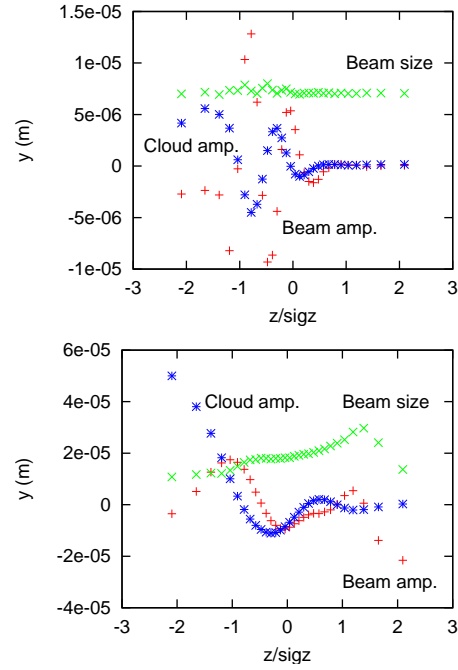


Figure 6: Beam and cloud centroid, and beam size along the longitudinal coordinate. Pictures (a) and (b) are given for  $\nu_s = 0$  and  $= 0.002$ .

such the beam enlargement. Actually the cloud is considered to distribute uniformly along the ring in most case. In this case this enlargement is false. This type of beam enlargement must be treated carefully in simulations. Anyway the threshold of the head-tail instability is given as  $\rho_e / \nu_s \sim 0.5 - 1 \times 10^{12} \text{ m}^{-3} / 0.01$  for the GLC/NLC-I damping ring. This threshold value is critical for 99.5% protection of photons but is serious for 99% protection.

The same simulation was performed for the second parameter, GLC/NLC-II. Figure 9 shows the growth of the beam size as a function of time (turn) for cloud densities  $\rho_e = 1$  and  $2 \times 10^{12} \text{ m}^{-3}$  and  $\nu_s = 0.0118$ . The threshold of the head-tail instability is given as  $\rho_e \sim 1 - 2 \times 10^{12} \text{ m}^{-3}$  for  $\nu_s = 0.0118$  at the GLC/NLC-II damping ring.

We next discuss for the TESLA damping ring. The TESLA damping ring has a long wiggler section with 500 m length. The cloud density of drift space is considered to be much less than that of wiggler section. In the simulation, feature of the instability is determined by the averaged cloud density integrated over the ring circumference,

$$\bar{\rho}_e = \frac{1}{L} \oint \rho_e(s) ds. \quad (14)$$

Beam is flat shape at arc and wiggler sections, while is round shape at drift section in the ring. Since the wiggler and arc section is dominant, the simulation is performed for flat beam. Figure 10 shows growth of the vertical beam size. We put 10 interaction point with electron cloud in the ring. This simulation is performed with the condition that electrons move freely: that is, electrons in drift space

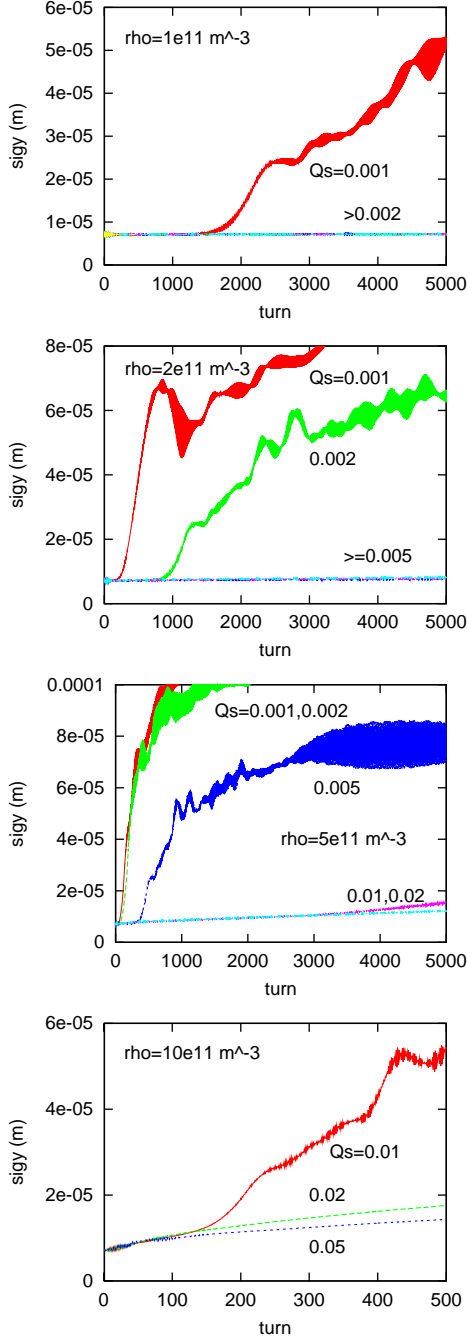


Figure 7: Growth of the beam size as a function of time (turn) for various cloud densities and synchrotron tunes at the GLC/NLC-I damping ring.

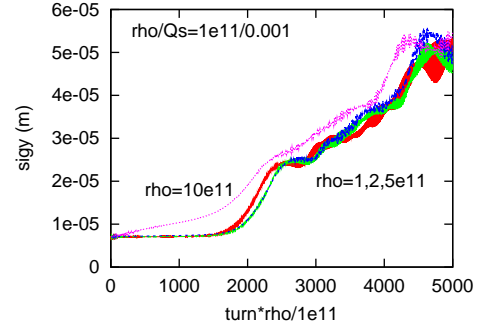


Figure 8: Scaling of the beam size growth.

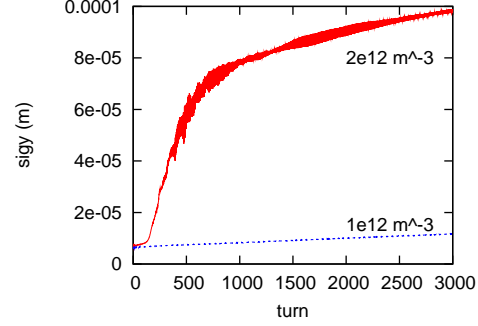


Figure 9: Growth of the beam size as a function of time (turn) for cloud densities  $\rho_e = 1$  and  $2 \times 10^{12} \text{ m}^{-3}$  and  $\nu_s = 0.0118$  at the GLC/NLC-II damping ring.

are taken into account. An evolution of the beam size for various cloud density is depicted in picture (a). The picture shows that beam enlargement is seen for cloud density  $\bar{\rho}_e \geq 5 \times 10^{10} \text{ m}^{-3}$ . The behavior for  $\bar{\rho}_e = 5 \times 10^{10} \text{ m}^{-3}$  is somewhat different from those of higher density. Picture (b) depicts the beam size evolution for 10 and 40 interaction points at the cloud density of  $\bar{\rho}_e = 5 \times 10^{10} \text{ m}^{-3}$ . The beam size growth disappears for 40 interaction points: that is, the growth, which is caused by localized distribution of cloud, may be false. Figure 11 shows growth of the vertical beam size in the condition that electrons move only vertical direction: i.e., motion in strong bending field is taken into account. The threshold, which is somewhat higher, is in the range of  $\bar{\rho}_e = 10 - 20 \times 10^{10} \text{ m}^{-3}$ .

We conclude the threshold density is in the range of  $\bar{\rho}_e = 5 - 10 \times 10^{10} \text{ m}^{-3}$  at the TESLA damping ring. If electrons in strong bending field dominate the instability, the threshold includes to  $\bar{\rho}_e = 10 - 20 \times 10^{10} \text{ m}^{-3}$ . The wiggler section occupies 3% of the whole ring, therefore the local density of the wiggler section should be less than  $\rho_{e,w} = 3 - 6 \times 10^{12} \text{ m}^{-3}$ , where the threshold for strong bending field is multiplied by 30. The neutral density estimated by the beam line density is  $\rho_{e,n} = 2 \times 10^{10} / (6 \times 0.032 \times 0.018) = 5.8 \times 10^{12} \text{ m}^{-3}$ , where the cross-section of wiggler chamber is  $32 \times 18 \text{ mm}^2$ . If the wiggler section, the cloud density is neutralized by multipactoring, the instability may be serious. Some care (for

example putting gaps in the train), may be required so that the density does not increase to the neutralization level.

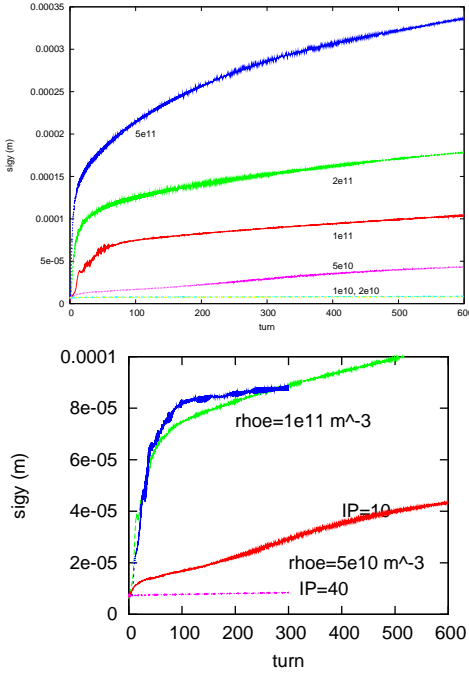


Figure 10: Evolution of the beam size for various cloud densities. Picture (a) is obtained for 10 interaction points with cloud. Picture (b) is obtained for 10 and 40 interaction points at cloud densities  $\rho_e = 5 \times 10^{10} \text{ m}^{-3}$  and  $1 \times 10^{11} \text{ m}^{-3}$ .

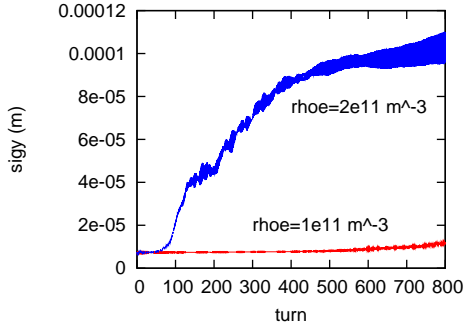


Figure 11: Evolution of the beam size for various cloud densities. Picture is obtained for 40 interaction points at cloud densities  $\rho_e = 1 \times 10^{11} \text{ m}^{-3}$  and  $2 \times 10^{11} \text{ m}^{-3}$ .

## SUMMARY

We have studied electron cloud effects in the GLC/NLC and partly in the TESLA damping rings. Multipactoring condition, in which electrons increase exponentially, was evaluated for drift section and bending magnet. The threshold value in drift space was  $\delta_{2,\text{max}} = 1.3$  for GLC/NLC-II and 1.9 for TESLA. In bending magnets, Amplification factor is 40-70 and 30-70 in drift section and bend-

ing magnets, respectively for  $\delta_{2,\text{max}} = 1.2 - 1.3$  in the GLC/NLC damping ring. Basically the threshold for the TESLA damping ring is higher than that for GLC/NLC. However since the train length is very long in the TESLA damping ring, some care (for example putting gaps in the train) may be required.

We estimated cloud density for the primary electron production rate  $n_e = 3.3 \times 10^{-4} / m \cdot e^+$  and secondary yield  $\delta_{2,\text{peak}} = 1.2$  in the GLC/NLC-II damping ring. Electron cloud is built up to the density of  $1.5 \times 10^{12} \text{ m}^{-3}$  at center and  $0.7 \times 10^{12} \text{ m}^{-3}$  in average, if 99.5% of the photoelectrons are protected by an antechamber.

The growth time of the coupled bunch instability was  $600 \mu\text{s}$  (600 turns) in the GLC/NLC-II damping ring. The growth can be cured by a bunch-by-bunch feedback system which can has capacity of damping time of about 100 turn.

The threshold of the single bunch instability was estimated by an analytical theory and tracking simulations. The threshold was estimated  $\rho_e = 2.9 \times 10^{12} \text{ m}^{-3}$  at  $\nu_s = 0.01$  and  $\rho_e = 6.2 \times 10^{12} \text{ m}^{-3}$  at  $\nu_s = 0.0118$  in the GLC/NLC-I and II damping rings, respectively by the analytic theory. Tracking simulations were done to determine more accurate threshold cloud density. Threshold of the single bunch instability was scaled by  $\rho_e / \nu_s$ . The scaled threshold was in the ranges of  $\rho_e / \nu_s = 0.5 - 1 \times 10^{12} / 0.01 \text{ m}^{-3}$  and  $1 - 2 \times 10^{12} / 0.01 \text{ m}^{-3}$  for the GLC/NLC-I and II, respectively. These threshold values had a discrepancy of factor 3-6 between analytical theory and tracking simulation. The discrepancy is not essential problem, but should be considered the limit of the linear theory. A large phase angle of electron motion in a bunch,  $\omega_c \sigma_z / c \geq 10$ , induces pinching or disruption of the cloud, with the result that the linear theory overestimates the threshold of the instability. Our conclusion for the single bunch instability is the values given by simulations,  $\rho_e / \nu_s = 0.5 - 1 \times 10^{12} / 0.01 \text{ m}^{-3}$  and  $1 - 2 \times 10^{12} / 0.01 \text{ m}^{-3}$  for the GLC/NLC-I and II, respectively. This threshold value is critical for 99.5% protection of photons but is serious for 99% protection.

The same analysis was performed for the TESLA damping ring. The analytic theory gave the threshold,  $2.2 \times 10^{11} \text{ m}^{-3}$ . The tracking simulation, in which electrons move freely, showed the threshold in the range of  $\bar{\rho}_e = 5 - 10 \times 10^{10} \text{ m}^{-3}$  for  $\nu_s = 0.065$ . The simulation, in which electrons move in strong bending magnetic field, showed the higher threshold,  $\bar{\rho}_e = 10 - 20 \times 10^{10} \text{ m}^{-3}$ . Here we use  $\bar{\rho}_e$  (Eq.14), because the cloud density strongly depends on section in the TESLA damping ring. The simulation for free electrons have again discrepancy of factor 2-4 due to the large phase angle  $\omega_c \sigma_z / c = 12$ , while that in bending magnet is roughly consistent with the linear theory. In the strong magnetic field, electrons are pinched only along the vertical direction, therefore it is understood that the simulation in bending field showed better consistency.

The wiggler section occupies 3% of the whole ring, therefore the local density of the wiggler section should be less than  $\rho_{e,w} = 3 - 6 \times 10^{12} \text{ m}^{-3}$ . Probably the head-

tail instability does not occur, if some cares, for example putting gaps in the train, are done so that the cloud density does not increase up the neutralization level in magnets.

## ACKNOWLEDGMENTS

The author thanks M. Pivi, K. Yokoya and F. Zimmermann for fruitful discussions.

## REFERENCES

- [1] J. Jowett, H. Owen, F. Zimmermann, Proceedings of the PAC2001, 4065 (2001).
- [2] A. Wolski, Proceedings of ELOUD02.
- [3] K. Ohmi, Proceedings of ELOUD02.
- [4] M. Pivi et al., in this proceedings.
- [5] M. A. Furman and G. R. Lambertson, Proceedings of the PAC97, 1617 (1997).
- [6] K. Ohmi, Phys. Rev. Lett., **75**, 1526 (1995).
- [7] K. Kanazawa, private communications.
- [8] Y. Suetsugu, Proceedings of Ultra vacuum techniques for accelerators and storage rings, KEK-Proceedng-2004-1ZA, 107 (2004).
- [9] G. Arduini et al., Proceedings of ELOUD02.
- [10] S.S. Win et al., Proceedings of ELOUD02.
- [11] K. Ohmi, F. Zimmermann, E. Perevedentsev, Phys. Rev. E **65**, 16502 (2002).
- [12] K. Ohmi and F. Zimmermann, Phys. Rev. Lett., **85**, 3821 (2000).
- [13] Y. Cai, Proceedings of ELOUD02.
- [14] Liu et al., Proceedings of APAC04.
- [15] K. Ohmi, Proceedings of PAC2001, 1895 (2001).
- [16] K. Ohmi, Phys. Rev. E **62**, 7287 (2000).
- [17] K. Yokoya, private communications.
- [18] E. Anderson et al., Proceedings PAC99, 1686 (1999).
- [19] J. Qiang et al., Phys. Rev. ST-AB **5**, 104402 (2002).
- [20] G. Rumolo et. al., Proceedings of PAC2001, 1889 (2001).
- [21] F. Zimmermann et. al., Proceedings of PAC2003 (2003).